Steel and Composite Structures, *Vol. 36, No. 1 (2020) 47-62*
DOI: https://doi.org/10.12989/scs.2020.36.1.047

Vibration behavior of trapezoidal sandwich plate with functionally graded-porous core and graphene platelet-reinforced layers

Di Liang[1], Qiong Wu[2], Xuemei Lu*[3] and Vahid Tahouneh**[4]

[1]*College of Mechanical Engineering, Saitama Institute of Technology, Saitama 369-0293, Japan.*
[2]*College of Mechatronic Engineering, Nanjing Forestry University, Nanjing 210037, China.*
[3]*School of International Education, Nanning Normal University, Nanning 530001, China.*
[4]*Young Researchers and Elite Club, Islamshahr Branch, Islamic Azad University, Islamshahr, Iran*

(*Received February 8, 2020, Revised June 5, 2020, Accepted June 10, 2020*)

Abstract. In this study, free vibration behavior of trapezoidal sandwich plates with porous core and two graphene platelets (GPLs) reinforced nanocomposite outer layers are presented. The distribution of pores and GPLs are supposed to be functionally graded (FG) along the thickness of core and nanocomposite layers, respectively. The effective Young's modulus of the GPL-reinforced (GPLR) nanocomposite layers is determined using the modified Halpin-Tsai micromechanics model, while the Poisson's ratio and density are computed by the rule of mixtures. The FSDT plate theory is utilized to establish governing partial differential equations and boundary conditions (B.C.s) for trapezoidal plate. The governing equations together with related B.C.s are discretized using a mapping- generalized differential quadrature (GDQ) method in the spatial domain. Then natural frequencies of the trapezoidal sandwich plates are obtained by GDQ method. Validity of current study is evaluated by comparing its numerical results with those available in the literature. A special attention is drawn to the role of GPLs weight fraction, GPLs patterns of two faces through the thickness, porosity coefficient and distribution of porosity on natural frequencies characteristics. New results show the importance of this permeates on vibrational characteristics of porous/GPLR nanocomposite plates. Finally, the influences of B.C.s and dimension as well as the plate geometry such as face to core thickness ratio on the vibration behaviors of the trapezoidal plates are discussed.

Keywords: trapezoidal sandwich plate; porosity; Generalized Differential Quadrature (GDQ); vibration; graphene platelets weight fraction

1. Introduction

Normally, functionally graded materials (FGMs) are heterogeneous materials in which the elastic and thermal properties change from one surface to the other, gradually and continuously. The material is constructed by smoothly changing the volume fraction of its constituent materials. FGMs offer great promise in applications where the operating conditions are severe, including spacecraft heat shields, heat exchanger tubes, plasma facings for fusion reactors, engine components, and high-power electrical contacts or even magnets. For example, in a conventional thermal barrier coating for high-temperature applications, a discrete layer of ceramic material is bonded to a metallic structure. However, the abrupt transition in material properties across the interface between distinct materials can cause large interlaminar stresses and lead to plastic deformation or cracking (Finot and Suresh 1996). These adverse effects can be alleviated by functionally grading the material to have a smooth spatial variation of material composition. The concept of FGMs was first introduced in Japan in 1984. Since then it has gained considerable attention (Koizumi 1993). A lot of different applications of FGMs can be found in (Zhu and Meng 1995). Owing to the superior properties against the conventional composite laminates, FGMs have found increasing applications in modern engineering designs, such as aircraft fuselage, rocking-motor casing, packaging materials in microelectronic industry, human implants, and so on. FG plates have extensive applications in different engineering branches. For mechanical engineering and aerospace engineering it can be used in different aircraft components such as turbine or fan blades, wings and also vacuum filter segment with replaceable sector plates. Mukhopadhyay (1979, 1982) used a semi-analytical method and Srinivasan and Thiruvenkatachari (1983, 1986) used the integral equation technique to analyze the vibrations of annular sector plates, respectively. Kim and Dickinson (1989) used one-dimensional (1-D) orthogonal polynomials and Liew and Lam (1993) used two-dimensional orthogonal polynomials as admissible functions to study the free vibration of annular sector plates by the Rayleigh-Ritz method. Seok and Tiersten (2004) used a variational approximation procedure to analyze the free vibration of cantilevered annular sector plates. Houmat (2001) used the hierarchical finite element method to study the free vibration of annular sector plates. Sharma and Marin (2013)

*Corresponding author, Research Assistant
E-mail: luixmei@126.com
**Corresponding author, Ph.D.,
E-mail: vahid.th1982@gmail.com

Copyright © 2020 Techno-Press, Ltd.
http://www.techno-press.org/?journal=scs&subpage=8
ISSN: 1229-9367 (Print), 1598-6233 (Online)

considered wave propagation in micropolar thermoelastic solid half space with distinct conductive and thermodynamic temperatures. Marin and Florea (2014) investigated porous micropolar bodies. Marin *et al.* (2013) studied nonsimple material problems considering Lagrange approach. The Lagrange identity method was developed by Marin (1994) to study the initial boundary value problem of thermoelasticity of bodies with microstructure. Sharma *et al.* (2005a, 2005b) integrated an analytical approach with the Chebyshev polynomials technique to study the buckling and free vibration of isotropic and laminated composite sector plates based on the first-order shear deformation theory. For moderate thickness plates, the first-order shear deformable plate theory is commonly used, which could provide a result more accurate than that from the CPT. In another studies (Marin and Nicaise 2016 and Marin *et al.* 2017) researchers studied different effects of porosity and voids in the material. Marin *et al.* (2019) formulated the mixed backward in time problem in the context of thermoelasticity for dipolar materials. To prove the consistency of this mixed problem, their first main result was regarding the uniqueness of the solution for this problem. This was obtained based on some auxiliary results, namely, four integral identities. The second main result was regarding the temporal behavior of our thermoelastic body with a dipolar structure. Barka *et al.* (2016) studied Thermal post-buckling behavior of imperfect temperature-dependent sandwich FG plates. Bouguenina *et al.* (2015) studied FG plates with variable thickness subjected to thermal buckling. Chen, Liu and Chen (2017) studied Vibration and stability of initially stressed sandwich plates with FGM face sheets. Wu and Liu (2016) developed a state space differential reproducing kernel (DRK) method in order to study 3D analysis of FG circular plates. Park *et al.* (2016) used modified couple stress for dynamic analysis of sigmoid functionally graded materials plates. Arefi (2015) suggested an analytical solution of a curved beam with different shapes made of functionally graded materials (FGMs). Bennai *et al.* (2015) developed a new refined hyperbolic shear and normal deformation beam theory to study the free vibration and buckling of functionally graded (FG) sandwich beams under various boundary conditions. Bouchafa *et al.* (2015) used refined hyperbolic shear deformation theory (RHSDT) for the thermoelastic bending analysis of functionally graded sandwich plates. Tahouneh (2016) presented a 3-D elasticity solution for free vibration analysis of continuously graded carbon nanotube-reinforced (CGCNTR) rectangular plates resting on two-parameter elastic foundations. The volume fractions of oriented, straight single-walled carbon nanotubes (SWCNTs) were assumed to be graded in the thickness direction. Moradi-Dastjerdi and Momeni-Khabisi (2016) studied Free and forced vibration of plates reinforced by wavy carbon nanotube (CNT). The plates were resting on Winkler-Pasternak elastic foundation and subjected to periodic or impact loading. Kamarian *et al.* (2015) studied vibration analysis of sandwich beams. The material properties of the FG nanocomposite sandwich beam are estimated using the Eshelby-Mori-Tanaka approach. Tornabene *et al.* (2016) investigated the effect of Carbon Nanotube (CNT) agglomeration on the free vibrations of laminated composite doubly-curved shells and panels reinforced by CNTs. Fantuzzi *et al.* (2017) studied free vibration of arbitrarily shaped FG carbon nanotube-reinforced plates using generalized differential quadrature method. Some additional parametric studies were also performed to analyze the effect of a mesh distortion, by considering several geometric and mechanical configurations. Tornabene *et al.* (2017) investigated the static response of composite plates and shells reinforced by agglomerated nanoparticles made of carbon nanotubes. A two-parameter agglomeration model was taken into account to describe the micromechanics of such particles, which showed the tendency to agglomerate into spherical regions when scattered in a polymer matrix. Saidi *et al.* (2013) used an analytical solution for thermomechanical bending analysis of functionally graded sandwich plates. The thermal buckling behavior of functionally graded sandwich plates was studied by Kettaf *et al.* (2013) via a new hyperbolic displacement model. Unlike any other theory, the theory was variationally consistent and gives four governing equations. Eyvazian *et al.* (2019) considered the instability behavior of sandwich plates considering magnetorheological (MR) fluid core and piezoelectric reinforced face sheets. Salah *et al.* (2019) used a simple four-variable integral plate theory that employed for examining the thermal buckling properties of functionally graded material (FGM) sandwich plates. The proposed kinematics considers integral terms which include the effect of transverse shear deformations. Sahla *et al.* (2019) use a simple four-variable trigonometric shear deformation model with undetermined integral terms to consider the influences of transverse shear deformation dynamic analysis of anti-symmetric laminated composite and soft core sandwich plates. The buckling analysis of micro sandwich plate with an isotropic/orthotropic cores and piezoelectric/polymeric nanocomposite face sheets was studied by Rajabi and Mohammadimehr (2019). In this research, two cases for core of micro sandwich plate is considered that involve five isotropic Deviney cell materials (H30, H45, H60, H100 and H200) and an orthotropic material also two cases for face sheets of micro sandwich plate is illustrated that include piezoelectric layers reinforced by carbon and boron-nitride nanotubes and polymeric matrix reinforced by carbon nanotubes under temperature-dependent and hydro material properties on the elastic foundations. The nonlinear behavior of steel sandwich panels, with different core materials: (1) Hollow (no core material); (2) Rigid Polyurethane Foam (RPF); and (3) Vulcanized Rubber (VR) under free air blast loads, was investigated using detailed 3D nonlinear finite element models in Ansys Autodyn (Rashad and Yang 2018). Tornabene *et al.* (2019) investigated free vibration analysis of arches and beams made of composite materials via a higher-order mathematical formulation. Tornabene *et al.* (2017) studied free vibration analysis of composite sandwich plates and doubly curved shells with variable stiffness. The reinforcing fibers were located in the external skins of the sandwich structures according to curved paths. A survey of several methods under the heading of strong formulation finite element method (SFEM) was presented by Tornabene *et al.*

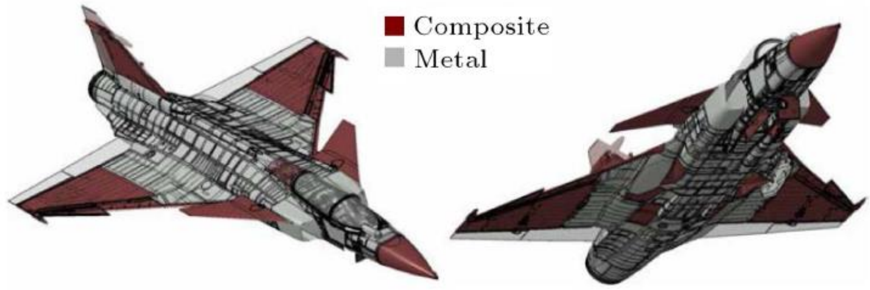

Fig. 1 Trapezoidal composite plates and components in JAS39 Gripen (Kapidzic 2013)

(2015). In another investigation CNT/epoxy nanocomposite have been fabricated by in situ polymerization technique and piezoresistive responses of the samples have been recorded and evaluated (Afrookhteh *et al.*, 2016). The 3D microstructure of the gas diffusion layers (GDLs) was generated, using a stochastic reconstruction approach. The method used basic input parameters and fibers orientation distribution and was capable to model carbon fiber and binder phases of all types of carbon fiber GDLs with different structural parameters (Afrookhteh *et al.*, 2016).

Trapezoidal plates are used commonly as structural components in many engineering applications such as ships, aircraft, and engineering construction (Fig. 1). Many researchers have investigated the free vibration behavior of trapezoidal plates. Gürses *et al.* (2009) used discrete singular convolution (DSC) method for the free vibration analysis of laminated trapezoidal plates. The differential quadrature (DQ) method in conjunction with the introduced transformed weighing coefficients (TW-DQ) was formulated to solve geometrically nonlinear free vibration of functionally graded carbon nanotube-reinforced composite (FG-CNTRC) quadrilateral plates (Setoodeh and Shojaee 2016). Gupta and Sharma (2014) investigated free transverse vibration of orthotropic thin trapezoidal plate of parabolically varying thickness in x-direction subjected to linear temperature distribution in x-direction through a numerical method. Zamani *et al.* (2012) studied free vibration analysis of moderately thick symmetrically laminated general trapezoidal plates with various combinations of boundary conditions. The governing partial differential equations and boundary conditions for trapezoidal plate are obtained using first order shear deformation theory (FSDT) together with proper transformation from Cartesian system into trapezoidal coordinates. Generalized differential quadrature (GDQ) method is then employed to obtain solutions for the governing equations. Torabi and Afshari (2017) investigated vibration analysis of cantilevered non-uniform trapezoidal thick plates based on the first shear deformation theory. Convergence and accuracy of the proposed solution were confirmed using results presented by other authors and also results obtained based on the finite element method using ANSYS software. Gupta and Sharma (2016) investigated free transverse vibrations of non-homogeneous trapezoidal plates of linear thickness variation in the x-direction under thermal gradient effect. The non-homogeneity of the plate was assumed to arise due to parabolic density variation in the y-direction. A two term deflection function has been taken for clamped-simply supported-clamped-simply supported boundary conditions. A general variational formulation for free vibration analysis of hybrid (metal composite) plates with a trapezoidal platform was presented by Shokrollahi and Shafaghat (2016). The plate was composed of two distinguished parts in the span direction, where the inboard section was assumed to be made of an isotropic metal, and the outboard section was from a laminated composite material. Zhao *et al.* (2017) studied bending and vibration behaviors of a novel class of functionally graded trapezoidal plates reinforced with graphene nanoplatelets (GPLs) by employing the finite element method. Modified Halpin-Tsai model and the rule of mixture were used to determine the effective material properties including Young's modulus, mass density and Poisson's ratio of the nanocomposites. Zhao *et al.* (2019) studied bending behaviours of functionally graded trapezoidal nanocomposite plates reinforced with graphene platelets (GPLs) under thermo-mechanical loading by employing finite element method. Analysis of FG-CNTR plates were first presented by Shen (2009) in which he studied the nonlinear bending behavior of FG-CNTR plates in thermal environment. He concluded that the load bending moment curves of the plate could be significantly increased as a result of functionally graded CNT reinforcements. Shen and Zhang (2010) presented thermal buckling and post buckling behavior of functionally graded nanocomposite plates reinforced by single-walled carbon nanotubes (SWCNTs). In comparison with research works on the free vibration or buckling analyses of FG structures, only a few references can be found that consider the effect of waviness and aspect ratio on the free vibrational behavior of panels with four edges simply supported (Moradi-Dastjerdi, Foroutan, and Pourasghar 2013). Moradi-Dastjerdi, Foroutan, and Pourasghar (2013) investigated the effects of CNT waviness on the dynamic behavior of FG-CNTR cylinder under impact load.

To the best of authors' knowledge, no papers have been reported in the literature concerning the vibrational behavior of the trapezoidal sandwich porous/GPLR plates with various combinations of B.C.s. In this study, sandwich plates with metallic foam core and two (GPLs) reinforced nanocomposite outer layers were proposed as lightweight engineering structures. Using GDQ method, the free

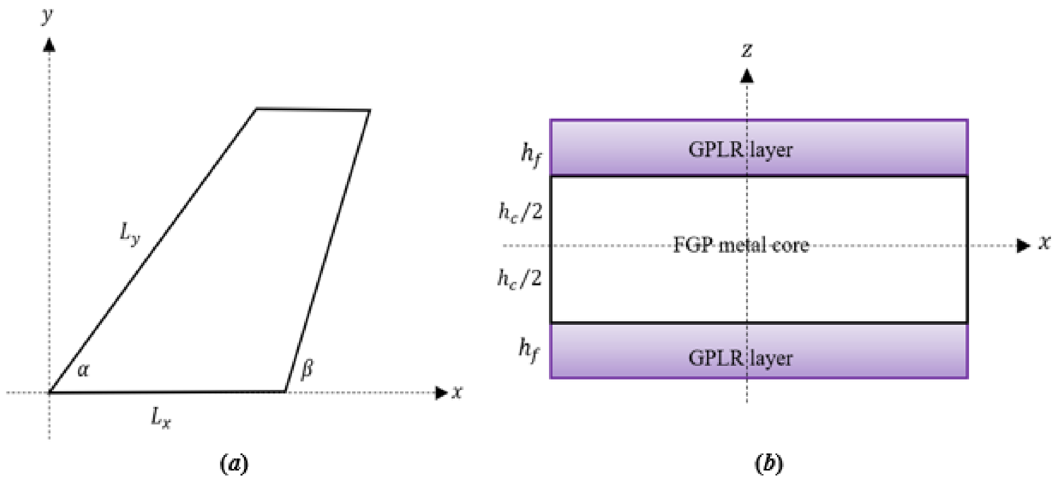

Fig. 2 Trapezoidal sandwich plates with FG porous core and two nanocomposite outer layers reinforced with GPLs. (*a*) top view, (*b*) side view

vibration analysis of three-layer sandwich plates with porous core is investigated and natural frequencies of the trapezoidal sandwich plates are obtained.

2. Theoretical modeling

As shown in Fig. 2 A three-layer trapezoidal sandwich plate with thickness h in z direction, two lengths Lx and Ly and two angles α and β in the x-y plane, is considered. The sandwich plate consists of porous metal foam core and two face layers reinforced functionally with GPLs. The plate has total thickness h ($=h_c+2h_f$), where h_c and h_p are the thicknesses of the core and GPL reinforced layers, respectively. Superscript f and c, respectively, stand for the face layers and the porous core. It is supposed that the orthogonal Cartesian system located on the middle surface of the plate. Furthermore, the porosities and GPLs are distributed along the core and two face sheet thickness, respectively.

2.1 Effective material properties

Fig. 3 depicts three the porosity distributions of the core layer and three GPL dispersion patterns along the thickness direction of the face layers of plates. In addition, Fig. 3 demonstrates the distribution of GPLs in which three different GPLs distribution patterns are plotted. The variation of Young's modulus (E_m), shear modulus (G_m) and mass density (ρ_m) through the thickness of metal foam core layer ($-h_c/2 \le z \le h_c/2$) corresponding to three different types of porosity distributions are explicitly formulated as (Wang *et al*. 2019):

$$\begin{aligned} E_c(z) &= E_m(1-e_0\lambda(z)) \\ G_c(z) &= G_m(1-e_0\lambda(z)) \\ \rho_c(z) &= \rho_m(1-e_1\lambda(z)) \end{aligned} \tag{1}$$

In which E_m and ρ_m are the maximum values of the Young's modulus and the mass density of the metallic porous core, respectively. λ(z) is formulated for each porosity pattern as follows (Zhao *et al.* 2019)

$$\lambda(z) = \begin{cases} 1-cos\left(\frac{\pi z}{h_c}\right) & FGP-1 \\ cos\left(\frac{\pi z}{h_c}\right) & FGP-2 \\ \lambda_0 & FGP-3 \end{cases} ; \quad \left(|z| \le \frac{h_c}{2}\right) \tag{2}$$

Also, the porosity coefficient $e_0 = 1-\frac{E_m}{E_0}$, $(0 < e_0 < 1)$ and $e_1 = 1-\frac{\rho_m}{\rho_0}$ is the coefficient mass density, where E_0 and ρ_0 are the minimum values of the Young's modulus and the mass density of the core, respectively. The relation between e_1 and e_0 can be expressed as

$$e_1 = 1-\sqrt{1-e_0} \tag{3}$$

Moreover, the term λ_0 which is implemented can be calculated by

$$\lambda_0 = \frac{1}{e_0} - \frac{1}{e_0}\left[\frac{2}{\pi}\sqrt{1-e_0} - \frac{2}{\pi} + 1\right]^2 \tag{4}$$

The variations of the Poisson's ratio are small enough to be considered unimportant. So, the poison's ratio is constant. It is assumed that two face layers are reinforced with three different GPLs distribution patterns without porous and the matrix and GPLs nanofillers are in perfect bond. Based on Halpin-Tsai micromechanical scheme, the effective Young's modulus of the two face sheets is (Rafiee *et al*. 2009):

$$E_f(z) = E_m\left[\frac{3}{8}\left(\frac{1+\xi_L\eta_L V_{GPL}}{1-\eta_L V_{GPL}}\right) + \frac{5}{8}\left(\frac{1+\xi_B\eta_B V_{GPL}}{1-\eta_B V_{GPL}}\right)\right] \tag{5}$$

where the subscripts 'GPL' and 'm' represent the corresponding material properties of the GPLs nanofillers and metallic matrix of face sheets, respectively. ξ_L, ξ_B, η_L, and η_B are geometrical parameters of the GPLs with the following expressions

$$\xi_L = 2\frac{L_{GPL}}{t_{GPL}}\ , \qquad \eta_L = \frac{E_{GPL}/E_m - 1}{E_{GPL}/E_m + \xi_L}\ ,$$
$$\xi_B = 2\frac{b_{GPL}}{t_{GPL}}\ , \qquad \eta_B = \frac{E_{GPL}/E_m - 1}{E_{GPL}/E_m + \xi_B}\ , \tag{6}$$

where L_{GPL}, b_{GPL}, and t_{GPL} are the GPLs' average length, width, and thickness, respectively. The effective Poisson's ratio, mass density can be estimated by the rule of mixtures.

$$\upsilon_f(z) = \upsilon_{GPL}V_{GPL} + \upsilon_m(1 - V_{GPL})$$
$$\rho_f(z) = \rho_{GPL}V_{GPL} + \rho_m(1 - V_{GPL}) \tag{7}$$

Then we define the following functions in terms of z to characterize the distributions of GPLs in which three GPL patterns are denoted by shape functions Θ(z) correspondingly

$$\Theta(z) = \begin{cases} 1 - cos\left(\dfrac{\pi\left(z - \frac{h_c}{2}\right)}{h_p}\right) & GPL-S \\ 1 - cos\left(\dfrac{\pi\left(z - \frac{h_c}{2}\right)}{2h_p} + \dfrac{\pi}{4}\right) & GPL-A \\ 1 & GPL-U \end{cases} \quad ; \quad \frac{h_c}{2} \le |z| \le \frac{h_c}{2} + h_f \tag{8}$$

The relationship between the shape functions $\Theta(z)$ and the volume fraction V_{GPL} of GPLs is

$$V_{GPL} = V_i\Theta_i(z) \tag{9}$$

where the peak values V_i , (i = 1, 2, 3) of the GPLs' volume fraction are functions of Λ_{GPL}. They are expressed by (Dong *et al.* 2019)

$$\frac{V_i}{h_f}\left(\int_{\frac{h_c}{2}}^{\frac{h_c}{2}+h_f} \Theta_i(z)dz\right) = \frac{\Lambda_{GPL}\rho_m}{\Lambda_{GPL}\rho_m + \rho_{GPL} - \Lambda_{GPL}\rho_m} \tag{10}$$

2.2 Governing equations and Boundary condition

According to the FSDT, the governing equations of motion for free vibration analysis of any symmetrically sandwich plate in Cartesian coordinate system are (Reddy 2003)

$$k_sA_{55}\left(\frac{\partial\varphi_x}{\partial x} + \frac{\partial^2 w}{\partial x^2}\right) + k_sA_{44}\left(\frac{\partial\varphi_y}{\partial y} + \frac{\partial^2 w}{\partial y^2}\right) = I_0\frac{\partial^2 w}{\partial t^2}$$
$$D_{11}\frac{\partial^2\varphi_x}{\partial x^2} + D_{12}\frac{\partial^2\varphi_y}{\partial y\partial x} + D_{66}\left(\frac{\partial^2\varphi_x}{\partial y^2} + \frac{\partial^2\varphi_y}{\partial y\partial x}\right) - k_sA_{55}\left(\varphi_x + \frac{\partial w}{\partial x}\right) = I_2\frac{\partial^2\varphi_x}{\partial t^2} \tag{11}$$
$$D_{22}\frac{\partial^2\varphi_y}{\partial y^2} + D_{12}\frac{\partial^2\varphi_x}{\partial y\partial x} + D_{66}\left(\frac{\partial^2\varphi_y}{\partial x^2} + \frac{\partial^2\varphi_x}{\partial y\partial x}\right) - k_sA_{44}\left(\varphi_y + \frac{\partial w}{\partial y}\right) = I_2\frac{\partial^2\varphi_y}{\partial t^2}$$

In which the displacement components of the trapezoidal plate along z directions are illustrated by w at middle surface. ψ_x and ψ_y separately, denote rotational displacements about the x- and y- axis. Besides, k_s is the shear correction factor which is assumed to be 5/6, other coefficients are defined as

$$\{A_{ij}, D_{ij}\} = \left(\int_{\frac{h_c}{2}}^{h_f+\frac{h_c}{2}} Q_{ij}(1, z^2)dz + \int_{\frac{-h_c}{2}}^{\frac{h_c}{2}} \tilde{Q}_{ij}(1, z^2)dz + \int_{-(h_f+h_c/2)}^{\frac{-h_c}{2}} Q_{ij}(1, z^2)dz\right) \tag{12}$$

In which the coefficients of Q_{ij} and $\tilde{Q}_{ij}$ are the plane stress-reduced stiffness of the face layers and the porous core respectively; defined as bellow (Li *et al.* 2018)

$$Q_{11} = Q_{22} = \frac{E_f(z)}{1 - \upsilon_f(z)^2}\ ; \tilde{Q}_{11} = \tilde{Q}_{22} = \frac{E_c(z)}{1 - \upsilon_c{}^2}$$
$$Q_{12} = Q_{21} = \frac{\upsilon_f(z)E_f(z)}{1 - \upsilon_f(z)^2}\ ;\ \tilde{Q}_{12} = \tilde{Q}_{21} = \frac{\upsilon_c E_c(z)}{1 - \upsilon_c{}^2} \tag{13}$$
$$Q_{44} = Q_{55} = Q_{66} = G_f(z);\ \ \tilde{Q}_{44} = \tilde{Q}_{55} = \tilde{Q}_{66} = G_c(z)$$

Moreover, M_{ij} and Q_i are elements of resultant moment and shear force vectors in the Cartesian coordinates which are defined as

$$\begin{Bmatrix} M_{xx} \\ M_{yy} \\ M_{xy} \end{Bmatrix} = \begin{bmatrix} D_{11} & D_{12} & 0 \\ D_{12} & D_{22} & 0 \\ 0 & 0 & D_{66} \end{bmatrix} \begin{Bmatrix} \dfrac{\partial\varphi_x}{\partial x} \\ \dfrac{\partial\varphi_y}{\partial y} \\ \dfrac{\partial\varphi_y}{\partial x} + \dfrac{\partial\varphi_x}{\partial y} \end{Bmatrix} \tag{14}$$

$$\begin{Bmatrix} Q_x \\ Q_y \end{Bmatrix} = \begin{bmatrix} A_{55} & 0 \\ 0 & A_{44} \end{bmatrix} \begin{Bmatrix} \varphi_x + \dfrac{\partial w}{\partial x} \\ \varphi_y + \dfrac{\partial w}{\partial y} \end{Bmatrix} \tag{15}$$

Different boundary conditions for a random edge whose normal and tangential directions are denoted by n and s are as (Malekzadeh and Karami 2005)

$$\text{Free (F):}\ \mathrm{M_n = Q_n = M_{ns} = 0}$$
$$\text{Simply supported (S):}\ \ \mathrm{M_n} = \upvarphi_\mathrm{s} = \mathrm{w} = 0 \tag{16}$$
$$\text{Clamped (C):}\ \upvarphi_\mathrm{n} = \upvarphi_\mathrm{s} = \mathrm{w} = 0$$

where $\mathrm{M_n}$ and $\mathrm{M_{ns}}$ are resultant bending and twisting moments, respectively and $\mathrm{Q_n}$ is resultant shear force acting on the boundary in the z direction. Furthermore, φ_n and φ_s are rotations of the normal to the mid-plane in the plane n_z (normal plane) and s_z (tangent plane), respectively. These parameters can be defined in Cartesian coordinate as

$$\varphi_s = -n_y\varphi_x + n_x\varphi_y$$
$$\varphi_n = n_y\varphi_y + n_x\varphi_x$$
$$M_n = M_{xx}n_x{}^2 + M_{yy}n_y{}^2 + 2M_{xy}n_xn_y \tag{17}$$
$$M_{ns} = n_xn_y\left(M_{yy} - M_{xx}\right) + M_{xy}\left(n_x{}^2 - n_y{}^2\right)$$
$$Q_n = n_xQ_x + n_yQ_y$$

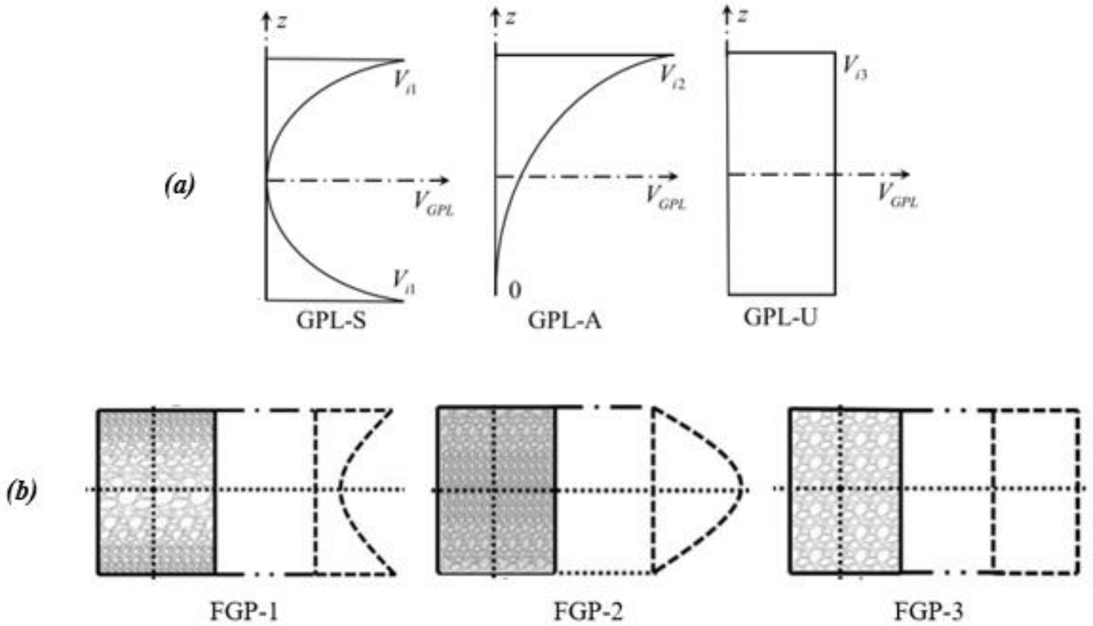

Fig. 3 Schematic of (a) The GPL dispersion patterns and (b) Different porosity distributions.

$$
\begin{aligned}
\varphi_s &= -n_y\varphi_x + n_x\varphi_y \\
\varphi_n &= n_y\varphi_y + n_x\varphi_x \\
M_n &= M_{xx}{n_x}^2 + M_{yy}{n_y}^2 + 2M_{xy}n_x n_y \\
M_{ns} &= n_x n_y\left(M_{yy} - M_{xx}\right) + M_{xy}\left({n_x}^2 - {n_y}^2\right) \\
Q_n &= n_x Q_x + n_y Q_y
\end{aligned}
\tag{17}
$$

where n_x and n_y are the x and y components of the vector normal to the edge, respectively.

2.3 Geometric mapping

The trapezoidal plate in the physical domain described in the Cartesian x-y coordinate system can be mapped into the computational domain described in the rectangular $\zeta - \eta$ coordinate system, the transformation equations are expressed as

$$
\begin{aligned}
x &= \zeta + \eta\cos(\alpha) - \frac{\eta\zeta\sin(\beta-\alpha)}{L_x\sin(\beta)} \\
y &= \eta\sin(\alpha)
\end{aligned}
\tag{18}
$$

the first-order and second-order derivatives of a function can be expressed in new $\zeta - \eta$ rectangular coordinates using the chain rule, as follows

$$
\begin{Bmatrix} \dfrac{\partial V}{\partial x} \\ \dfrac{\partial V}{\partial y} \end{Bmatrix} = [j]^{-1} \begin{Bmatrix} \dfrac{\partial V}{\partial \zeta} \\ \dfrac{\partial V}{\partial \eta} \end{Bmatrix}
\tag{19}
$$

$$
\begin{Bmatrix} \dfrac{\partial^2 V}{\partial x^2} \\ \dfrac{\partial^2 V}{\partial y^2} \\ \dfrac{\partial^2 V}{\partial x\partial y} \end{Bmatrix} = \left[j^{(2)}\right]^{-1} \begin{Bmatrix} \dfrac{\partial^2 V}{\partial \zeta^2} \\ \dfrac{\partial^2 V}{\partial \eta^2} \\ \dfrac{\partial^2 V}{\partial \zeta\partial \eta} \end{Bmatrix} - \left[j^{(2)}\right]^{-1}\left[j^{(1)}\right][j]^{-1} \begin{Bmatrix} \dfrac{\partial V}{\partial \zeta} \\ \dfrac{\partial V}{\partial \eta} \end{Bmatrix}
\tag{20}
$$

In which V stands for an arbitrary variable and the components of the transformation Jacobian matrices are

$$
[j] = \begin{bmatrix} \dfrac{\partial x}{\partial \zeta} & \dfrac{\partial y}{\partial \zeta} \\ \dfrac{\partial x}{\partial \eta} & \dfrac{\partial y}{\partial \eta} \end{bmatrix}; \quad \left[j^{(1)}\right] = \begin{bmatrix} \dfrac{\partial^2 x}{\partial \zeta^2} & \dfrac{\partial^2 y}{\partial \zeta^2} \\ \dfrac{\partial^2 x}{\partial \eta^2} & \dfrac{\partial^2 y}{\partial \eta^2} \\ \dfrac{\partial^2 x}{\partial \zeta\partial \eta} & \dfrac{\partial^2 x}{\partial \zeta\partial \eta} \end{bmatrix}
\tag{21}
$$

$$
\left[j^{(2)}\right] = \begin{bmatrix} \left(\dfrac{\partial x}{\partial \zeta}\right)^2 & \left(\dfrac{\partial y}{\partial \zeta}\right)^2 & 2\dfrac{\partial x}{\partial \zeta}\dfrac{\partial y}{\partial \zeta} \\ \left(\dfrac{\partial x}{\partial \eta}\right)^2 & \left(\dfrac{\partial y}{\partial \eta}\right)^2 & 2\dfrac{\partial x}{\partial \eta}\dfrac{\partial y}{\partial \eta} \\ \dfrac{\partial x}{\partial \zeta}\dfrac{\partial x}{\partial \eta} & \dfrac{\partial y}{\partial \zeta}\dfrac{\partial y}{\partial \eta} & \dfrac{\partial x}{\partial \zeta}\dfrac{\partial y}{\partial \eta} + \dfrac{\partial x}{\partial \eta}\dfrac{\partial y}{\partial \zeta} \end{bmatrix}
\tag{22}
$$

Based on the above transformation Jacobian matrix, the governing equations and boundary conditions can be transformed from the physical domain into the new computational domain. Using Eqs. (11) and (19), (20) one can obtain the governing equations of motion of sandwich trapezoidal plate in the $\zeta - \eta$ coordinate as

$$k_s A_{55}(b_1 \frac{\partial \varphi_x}{\partial \zeta} + k_{11} \frac{\partial^2 w}{\partial \zeta^2}) + k_s A_{44}(b_3 \frac{\partial \varphi_y}{\partial \zeta} + b_4 \frac{\partial \varphi_y}{\partial \eta} + k_{21} \frac{\partial^2 w}{\partial \zeta^2} + k_{22} \frac{\partial^2 w}{\partial \eta^2} + k_{23} \frac{\partial^2 w}{\partial \eta \partial \zeta} - a_{21} \frac{\partial w}{\partial \zeta}) = I_0 \frac{\partial^2 w}{\partial t^2} \tag{23}$$

$$\begin{gathered} D_{11}(k_{11} \frac{\partial^2 \varphi_x}{\partial \zeta^2}) + (D_{12} + D_{66})(k_{31} \frac{\partial^2 \varphi_y}{\partial \zeta^2} + k_{32} \frac{\partial^2 \varphi_y}{\partial \eta^2} + k_{33} \frac{\partial^2 \varphi_y}{\partial \zeta \partial \eta} - a_{31} \frac{\partial \varphi_y}{\partial \zeta}) + D_{66}(k_{21} \frac{\partial^2 \varphi_x}{\partial \zeta^2} + k_{22} \frac{\partial^2 \varphi_x}{\partial \eta^2} + \\ k_{23} \frac{\partial^2 \varphi_x}{\partial \eta \partial \zeta} - a_{21} \frac{\partial \varphi_x}{\partial \zeta}) - k_s A_{55}(\varphi_x + b_1 \frac{\partial w}{\partial \zeta}) = I_2 \frac{\partial^2 \varphi_x}{\partial t^2} \end{gathered} \tag{24}$$

$$\begin{gathered} D_{66}(k_{11} \frac{\partial^2 \varphi_y}{\partial \zeta^2}) + (D_{12} + D_{66})(k_{31} \frac{\partial^2 \varphi_x}{\partial \zeta^2} + k_{32} \frac{\partial^2 \varphi_x}{\partial \eta^2} + k_{33} \frac{\partial^2 \varphi_x}{\partial \zeta \partial \eta} - a_{31} \frac{\partial \varphi_x}{\partial \zeta}) + D_{22}(k_{21} \frac{\partial^2 \varphi_y}{\partial \zeta^2} + k_{22} \frac{\partial^2 \varphi_y}{\partial \eta^2} + \\ k_{23} \frac{\partial^2 \varphi_y}{\partial \eta \partial \zeta} - a_{21} \frac{\partial \varphi_y}{\partial \zeta}) - k_s A_{44}(\varphi_y + b_3 \frac{\partial w}{\partial \zeta} + b_4 \frac{\partial w}{\partial \eta}) = I_2 \frac{\partial^2 \varphi_y}{\partial t^2} \end{gathered} \tag{25}$$

in which:

$$\begin{gathered} b_1 = [j]^{-1}(1,1),\ b_3 = [j]^{-1}(2,1),\ b_4 = [j]^{-1}(2,2), \\ k_{mn} = [j^{(2)}]^{-1}(m,n), \\ a_{mn} = [j^{(2)}]^{-1}[j^{(1)}][j]^{-1}(m,n) \end{gathered} \tag{26}$$

It should be noted that boundary conditions also can be transformed into the computational domain using Eqs. (16) and (19)-(20).

3. Solution procedure

Differential quadrature method (DQM) is an accurate and effective numerical method. The convergence and accuracy of results depends on the precision of weighting coefficients controlled by the number of grid points. The primary formulations of DQM, an algebraic equation system was employed to calculate weighting coefficients which determined the number of grid points. An explicit formulation for the weighting coefficients was later presented by Shu (2012) and led to GDQ. This method uses weighted linear combination of function values in the whole domain to approximate the function derivations with respect to the space variables. For instance, the nth-order derivative of variable V with respect to the ζ at point ζ_i is approximated as

$$V^{(n)}(\zeta_i) = \left(\frac{d^n V}{d\zeta^n}\right)\Bigg|_{\zeta=\zeta_i} = \sum_{j=1}^{N_\zeta} C_\zeta^{(n)}(i,j) V_j, \qquad (1 \le i \le N_\zeta) \tag{27}$$

where N_ζ is the total number of grid points in the ζ direction and $C_\zeta^{(n)}$ are weighting coefficients for the nth-order derivative. In the GDQ method, the global Lagrange interpolation polynomial is used for determination of the weighting coefficients as

$$\begin{gathered} g_j(\zeta) = \frac{M(\zeta)}{(\zeta - \zeta_j) M^{(1)}(\zeta_j)} \\ M(\zeta) = \prod_{k=1}^{N_\zeta} (\zeta - \zeta_k) \\ M^{(1)}(\zeta_j) = \prod_{k=1, k \ne j}^{N_\zeta} (\zeta_j - \zeta_k) \end{gathered} \tag{28}$$

it can be concluded that $M^{(1)}(\zeta)$ is the first derivation of $M(\zeta)$ Now, derivation from Eq. (28) leads to analytic expression for $C_\zeta^{(n)}(i,j)$ as:

$$\begin{gathered} C_\zeta^{(1)}(i,j) = g_j^{(1)}(\zeta_i), \qquad (1 \le i,j \le N_\zeta), i \ne j \\ C_\zeta^{(1)}(i,i) = -\sum_{j=1, j \ne i}^{N_\zeta} C_\zeta^{(1)}(i,j), \qquad (1 \le i \le N_\zeta) \end{gathered} \tag{29}$$

The higher order derivative weighting coefficients can be found using following recursive formulation

$$\begin{gathered} C_\zeta^{(n)}(i,j) = n\left(C_\zeta^{(1)}(i,j) C_\zeta^{(n-1)}(i,i) - \frac{C_\zeta^{(n-1)}(i,j)}{\zeta_i - \zeta_j}\right), \\ (1 \le i,j \le N_\zeta), i \ne j \\ C_\zeta^{(n)}(i,i) = \sum_{j=1, j \ne i}^{N_\zeta} C_\zeta^{(n)}(i,j), \qquad (1 \le i \le N_\zeta) \end{gathered} \tag{30}$$

the natural and simplest choice of grid points is equally spaced points in the direction of the coordinate axes of the computational field. It was proven that the non-uniform grid points give better results than equally spaced grid points do with the same number of grid points. Using Eq. (27), one may rewrite the governing equations in algebraic discretized form. For example, the discretized form of the first governing equation, Eq. (23), can be read as

$$k_sA_{55}(\sum_{i=1}^{N_\zeta}(b_1C_\zeta^{(1)}\varphi_{x_{i,k}}+k_{11}C_\zeta^{(2)}w_{i,k})+k_sA_{44}[\sum_{i=1}^{N_\zeta}(b_3C_\zeta^{(1)}\varphi_{y_{i,k}}+k_{21}C_\zeta^{(2)}w_{i,k}-a_{21}C_\zeta^{(1)}w_{i,k})+\sum_{j=1}^{N_\eta}(b4C_\eta^{(1)}\varphi_{y_{j,k}}+$$
$$k_{22}C_\eta^{(2)}w_{l,j})+\sum_{m=1}^{N_\zeta}\sum_{n=1}^{N_\eta}k_{23}C_\zeta^{(1)}C_\eta^{(1)}w_{m,n}]=I_0\frac{\partial^2 w}{\partial t^2},\quad l=2,...,N_\zeta-1,k=2,...,N_\eta-1 \tag{31}$$

In this paper, a non-uniform set of grid points is chosen as follows

$$\xi_i=\frac{L_\zeta}{2}\left(1-\cos\left(\frac{i-1}{N_\xi-1}\pi\right)\right) \tag{32}$$

L_ζ is the length in the ζ direction. Applying GDQ method on Eqs. (23-25) with the special combination of B.Cs, one can write the subsequent set of algebraic equations as $[K]\{q\}=[M]\{\partial^2 q/\partial t^2\}$. Where {q} is vector of system degree of freedoms including values of w, φ_x and φ_y at all nodes. In order to obtain the natural frequencies, the nodes on boundaries and internal domain of the plate are separated. Combination equations of motion and B.C equations can now be rewritten as (Tornabene and Viola 2008)

$$\left\{\begin{bmatrix}[K_{bb}] & [K_{bd}]\\ [K_{db}] & [K_{dd}]\end{bmatrix}\right\}\begin{Bmatrix}q_b\\ q_d\end{Bmatrix}=\begin{bmatrix}[0] & [0]\\ [0] & [M_{dd}]\end{bmatrix}\begin{Bmatrix}\partial^2 q_b/\partial t^2\\ \partial^2 q_d/\partial t^2\end{Bmatrix} \tag{33}$$

Here, subscripts d and b indicate domain and boundary nodes, respectively. For example, $[K_{db}]$ indicates the effects of boundary nodes on the vibration of domain nodes. Here we have:

Number of all nodes: N^2

Number of all nodes DOFs: $3N^2$

Num. of boundary nodes DOFs (N_b): $3(N-4)^2$

Num. of domain nodes DOFs (N_d): $3[N^2-(N-4)^2]$

So, in Eq. (33): The dimensions of $[K_{bb}]$ (or $[M_{bb}]$) matrix is equal to $N_d \times N_b$. The dimensions of $[K_{bd}]$ (or $[M_{bd}]$) matrix is equal to $N_b \times N_d$. The dimensions of $[K_{db}]$ (or $[M_{db}]$) matrix is equal to $N_b \times N_b$ and the dimensions of $[K_{dd}]$ and $[M_{dd}]$ matrices are equal to $N_d \times N_d$. Also we know $[M_{bb}]=[0]$, $[M_{bd}]=[0]$ and $[M_{db}]=[0]$. Consequently The dimensions of $\begin{bmatrix}[K_{bb}] & [K_{bd}]\\ [K_{db}] & [K_{dd}]\end{bmatrix}$ and $\begin{bmatrix}[0] & [0]\\ [0] & [M_{dd}]\end{bmatrix}$ matrices are equal to (3N×M) ×(3N×M).

Due to harmonic nature of the vibration, it is reasonable to assume that $\{q\}=\{Q(\zeta,n)\}e^{i\omega t}$; Where ω is natural frequency of the plate. Rearranging the quadrature analogs of field equations and boundary conditions inside the fabric of a generalized eigenvalue problem yield

$$\left\{\begin{bmatrix}[M_{dd}] & [0]\\ [0] & [0]\end{bmatrix}\omega^2+\begin{bmatrix}[K_{dd}] & [K_{db}]\\ [K_{bd}] & [K_{bb}]\end{bmatrix}\right\}\begin{Bmatrix}Q_d\\ Q_b\end{Bmatrix}=0 \tag{34}$$

Eq. (34) can be transformed to a standard eigenvalue problem as

$$\left[K_{dd}-K_{db}{K_{bb}}^{-1}K_{bd}+\omega^2[M_{dd}]\right]\{Q_d\}=0 \tag{35}$$

Finally, by solving the eigenvalue problem, the natural frequencies can be obtained.

4. Results and discussions

In this section, numerical results of the free vibration analyses of trapezoidal sandwich GPLR/FGP plates with different porosity coefficient, porosity distribution, GPL distribution, GPL weight fraction, B.Cs and geometrical parameters are presented through some examples. The boundary conditions of the plate are stated by the letter symbols, for instance, CFSC means a plate with edges $\zeta=0$ clamped (C), $\eta=0$ free (F), $\zeta=L_x$ simply supported (S) and $\eta=L_y$ clamped (C).

4.1 Verification

In order to verify the present approach, results are compared with some existing ones in the literature. The verification example is a symmetrically laminated isosceles trapezoidal plate, (see Fig. 4) Composite material properties used in this study are as: $(E_1,G)=(40E_2,0.6E_2),\nu_{12}=0.25$ $,\rho=2500$ Kg/m^3.Dimensionless natural frequency $\left(\Omega=\frac{\omega a^2}{h}\sqrt{\rho/E_2}\right)$ of SSSS and CCCC [0 90]$_s$ laminated trapezoidal plate for different values of b/a and h/a are presented in Table 1 . Results of FE method (Haldar and Manna 2003) and DSC method (Gürses *et al.* 2009) are also included in the table for comparison. A good agreement can be seen between results of the GDQ method and those available from literature.

Table 2 demonstrates the first three dimensionless natural frequencies Ω of a [30 60]$_s$ laminated (lay-up configurations) right trapezoidal (see Fig. 4) with L_x=1, L_y=0.5 at two corner angles and different boundary conditions, the obtained results also have good agreements with reported results in literature for the vibration analysis of composite plates. Besides results show that as the angle θ increased, dimensionless frequency reduced.

4.2 Convergence study

During detailed parametric studies in this section, the mechanical properties of the GPL and metal matrix constituents of the face layers and core are: E_m=68.3GPa, E_G=1.01TPa, ρ_G =1062 Kg/m^3, ρ_m=2706 Kg/m^3, v_m=0.34; v_G=0.86 with L_G=2.5 μm, b_G=1.5 μm, t_G=1.5 nm.

Table 1 Comparison of fundamental frequency of $[0\ \ 90]_s$ symmetric trapezoidal plate by Refs

B.C.	h/a	b/a	Haldar and Manna 2003	Gürses et al. 2009	Present
SSSS	0.1	0.4	23.91	24.06	24.14
		0.8	17.39	18.41	17.69
	0.2	0.4	15.44	15.46	15.82
		0.8	11.97	11.99	12.31
CCCC	0.1	0.4	30.95	31.08	31.65
		0.8	24.73	25.12	25.44
	0.2	0.4	17.45	17.56	18.14
		0.8	14.46	14.59	14.90

Table 2 Validation of first three frequencies for $[30\ \ 60]_s$ laminated right trapezoidal plate at various B.C and two different side angles

Θ	B.C.	Frequency					
		1st mode		2nd mode		3rd mode	
		Present	Zamani et al. 2012	Present	Zamani et al. 2012	Present	Zamani et al. 2012
45	CCCC	16.865	16.866	23.615	23.618	30.164	30.199
	SSSS	12.067	11.716	19.250	19.154	26.320	26.315
	CSCS	14.924	14.888	21.215	21.192	27.741	27.764
	CFCF	8.602	8.554	13.855	13.702	15.287	15.051
	CFSF	4.465	4.412	10.199	10.172	13.450	13.347
	CFFF	0.712	0.572	3.146	3.320	5.278	5.229
60	CCCC	14.723	14.723	20.692	20.692	26.998	27.014
	SSSS	10.126	9.842	16.709	16.687	23.483	23.464
	CSCS	11.915	11.886	18.608	18.608	25.014	25.023
	CFCF	6.974	6.924	8.706	8.582	12.906	12.872
	CFSF	3.786	3.741	7.619	7.585	9.982	9.961
	CFFF	0.646	0.601	2.780	2.858	4.784	4.789

Since the number of assumed grid points can affect the results, the convergence of the results with respect to N is studied. In Table 3 convergence of the GDQ method for the first three dimensionless natural frequencies of plate $\left(\Omega = \omega L_x{}^2\sqrt{\rho h/D_{11}}/\pi^2\right)$ is investigated with: L_x=L_y=1.5, α=120, β=45, h_c /L_x=0.1, h_f /h_c=0.75. In the case of FGP-3 and GPL-U sandwich plate in which the GPL weight fraction and porous coefficient are set to (Λ_{GPL}, e_0) = (1%, 0.2); Results are prepared for different B.C.s. The problem is solved with six different mesh sizes. From the results one can conclude that GDQ leads to accurate results even using a few grid points. Also, results show that as the number of grid points increased GDQ results are rapidly converged to the final values which show fast rate of convergence of the method. Thus, the mesh size of 14×14 is used in the next numerical examples.

4.3 Numerical results

Effect of the boundary conditions on the fundamental natural frequency of sandwich porous/GPLR skew sandwich plate (α=β), is presented in Fig. 5. The results are attained when the core has porosities diffused in pattern (FGP-1) with fraction of 0.4 and GPLs distributed in the two face sheets in pattern GPL-S with $\Lambda_{GPL} = 1\%$,The other parameters considered (L_x, L_y, h)=(1.5,1,0.2), h_f/h_c=0.75. It can be concluded that as the plate tends to the rectangular shape (α=90), natural frequency decreases.

Fig. 6 investigates the effect of bottom angle β on the natural frequency of trapezoidal sandwich plate at various B.C.s in which the other dimensions of the plate are fixed as (L_x, L_y, h) = (1,1,0.2), α=120, h_f/ h_c= 0.75. The results are attained when the sandwich plate has porosities diffused in pattern (FGP-1) with fraction of 0.4 and GPLs distributed in pattern GPL-S with $\Lambda_{GPL} = 1\%$. Apparently, fundamental frequency increases when the angle β increases. This indicates that the increase in bottom angle will increases the stiffness and natural frequency of the trapezoidal plate. Fig. 7 illustrate the effect of weight fraction of GPL reinforced face sheets on Fundamental frequency change of the sandwich plate with FSCS B.C.s. In this figure all three different GPL pattern are depicted and (L_x, L_y, h) =

Table 3 Effect of B.C on Convergence study for first four natural frequency of trapezoidal plate

B.C.	Number of grid points	Mode sequence			
		1st	2nd	3rd	4th
CCCC	6	1.4830	2.2216	3.0207	3.6919
	9	1.4457	2.1572	2.8472	3.1689
	12	1.4457	2.1526	2.8403	3.1621
	15	1.4457	2.1526	2.8402	3.1617
	18	1.4457	2.1526	2.8402	3.1617
CSCS	6	1.1054	1.9359	2.4083	3.3327
	9	1.0769	1.9040	2.3601	2.8509
	12	1.0760	1.8996	2.3560	2.8464
	15	1.0756	1.8995	2.3555	2.8458
	18	1.0754	1.8995	2.3552	2.8457
SSSS	6	0.8559	1.5349	2.2714	3.0229
	9	0.8556	1.5583	2.1994	2.5448
	12	0.8569	1.5567	2.1975	2.5413
	15	0.8571	1.5570	2.1978	2.5413
	18	0.8575	1.5570	2.1981	2.5414
CFCF	6	0.5189	1.1040	1.2744	1.8498
	9	0.4903	1.0525	1.2218	1.7188
	12	0.4886	1.0480	1.2167	1.7085
	15	0.4886	1.0478	1.2148	1.7072
	18	0.4884	1.0478	1.2139	1.7067
CFSF	6	0.2898	0.8074	1.0729	1.7284
	9	0.2962	0.7972	1.0506	1.4327
	12	0.2947	0.7928	1.0465	1.4283
	15	0.2950	0.7927	1.0458	1.4282
	18	0.2950	0.7927	1.0455	1.4283
CFFF	6	0.0796	0.4805	0.8562	0.9686
	9	0.0499	0.2704	0.8228	1.2118
	12	0.0808	0.3493	0.7390	1.0951
	15	0.0719	0.2056	0.3948	0.9142
	18	0.0786	0.2271	0.3818	0.9007

(1,1,0.2), (α, β) = (120,45), h_f/h_c=0.75 with FGP-1 porosity distribution at porosity value e_0=0.4 are also assumed. As shown in this figure the fundamental frequency rises as GPL weight fraction increases. Numerical results indicate that graphene platelets play a substantial role in the enhancement of the plate stiffness. Additionally, it can be illustrated that the highest and the lowest frequency parameters are corresponded to the GPL-S and GPL-U patterns, respectively.

The variation of fundamental frequency of sandwich plate versus the porosity coefficient of core is plotted in Figs.8 considering all three different porosity distribution with CFCF B.C.s and GPL-U for face sheets. In this figure, the parameters considered (L_x, L_y, h)= (1,1,0.15), (α, β)= (90,60), h_f/h_c=0.5; Λ_{GPL}=1%. As shown in this figure, the porosity coefficient and distribution have a remarkable influence on fundamental frequency. Also, it can be illustrated that the highest and lowest frequencies are corresponded to the FGP-2 and FGP-3 porosity distributions. Besides it is found that fundamental frequency of sandwich plate with symmetric porosity distribution increases by increasing the porosity coefficient. It is due the fact that the effect of mass density of host layer overcomes that of flexural rigidity when the pores are symmetrically distributed about the mid-plane of the core sheet. The first two frequency parameter (Ω) of trapezoidal sandwich porous/GPLR plate for various porosity distribution, different GPL patterns and two different B.Cs are presented in Table 4; in which the parameters considered that (L_x, L_y ,h)=(1,1,0.2), (α,β)=(60,30), h_f/h_c=0.5 and (Λ_{GPL},e_0)=(1%,0.4).

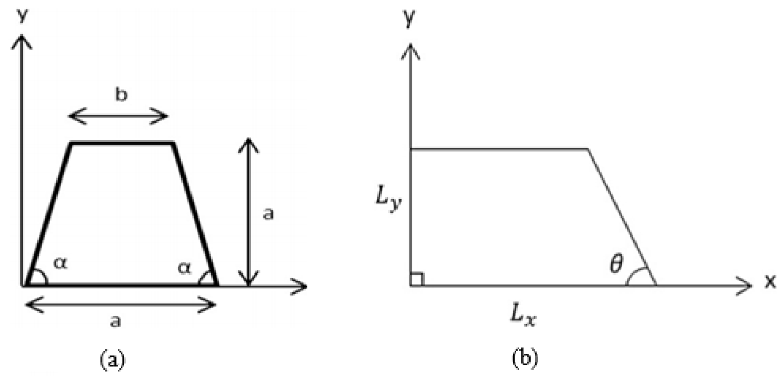

Fig. 4 Schematic view of: (a) symmetric trapezoidal plate and (b) right trapezoidal plate

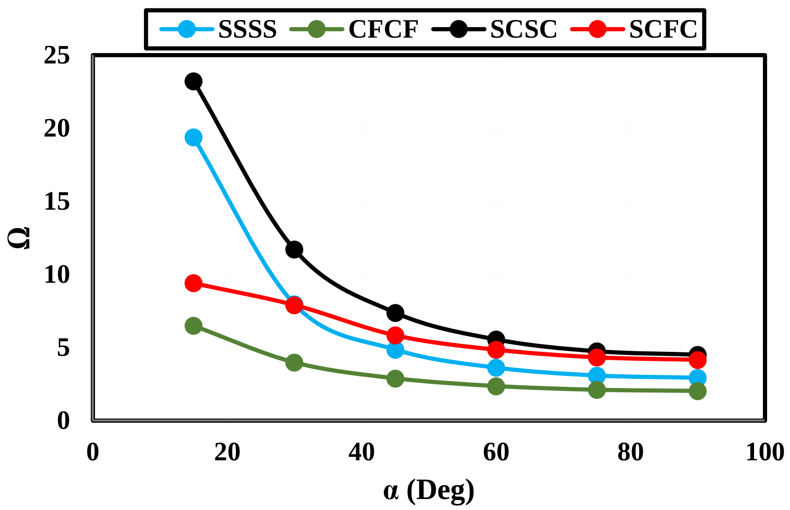

Fig. 5 Effect of bottom angles α on frequency parameters (Ω) of GPL/FGP skew sandwich plates at various B.Cs

Table 4. First two frequencies of trapezoidal sandwich porous/GPLR plate for different pattern of porosity and reinforced GPLs

B.C.	Pattern	1st mode			2nd mode		
		GPL-U	GPL-S	GPL-A	GPL-U	GPL-S	GPL-A
SSSS	FGP-3	1.9084	1.9678	1.9436	3.217	3.3754	3.3099
	FGP-2	1.9364	1.9955	1.9715	3.2595	3.4163	3.3515
	FGP-1	1.9236	1.9777	1.9557	3.2550	3.4003	3.3404
CFCF	FGP-3	1.2858	1.3525	1.3223	2.105	2.2796	2.2029
	FGP-2	1.3040	1.3698	1.3402	2.1305	2.3025	2.2272
	FGP-1	1.2999	1.3623	1.3341	2.1419	2.3061	2.2342

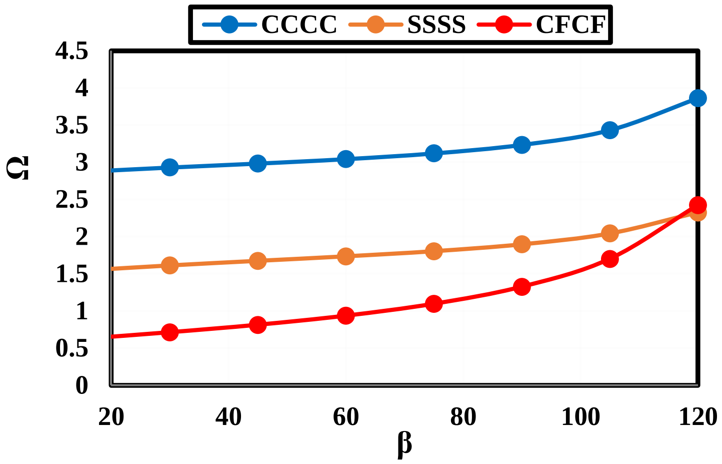

Fig. 6 Variation of Fundamental frequency parameter (Ω) of trapezoidal plate with its side degree, at various B.Cs

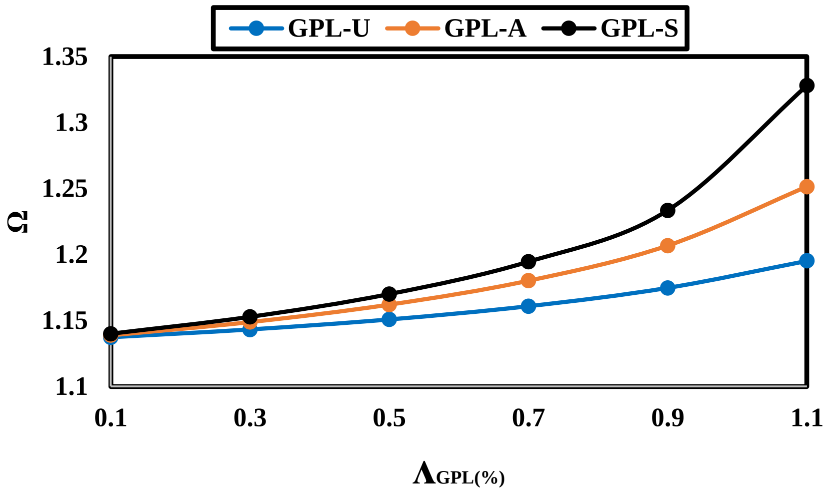

Fig. 7 Fundamental frequency parameter (Ω) of FSCS trapezoidal sandwich plate versus the GPL weight fraction at different reinforced patterns

This table shows that the max. Value of fundamental frequencies is relevant to FGP-2 porosity distribution together with GPL-S pattern.

Fig. 9 demonstrates the variation of fundamental frequency of CFSC sandwich plate as a function of face to core thickness ratio (h_f / h_c) for different GPL reinforced patterns. The parameters (L_x, L_y, h_c) = (1,1.5,0.1), (α, β) = (135,120) are assumed and that the core thickness of plate is kept constant. The results are obtained when the sandwich plate has porosities diffused in pattern (FGP-3) with fraction of 0.4 and GPLs distributed with $\Lambda_{GPL} = 1\%$. It can be seen that the frequency parameter of the sandwich plate decrease with the increase of the thickness ratio. Similar to the trend as observed in Fig. 6, plates with distribution pattern GPL-U has the smallest frequency while pattern GPL-S has the largest one. In addition, the variation of the dimensionless amplitude is found to be more sensitive to the thickness ratio for plates with pattern GPL-U than those with pattern GPL-A and pattern GPL-S.

5. Conclusions

This article is organized to investigate the vibrational characteristics of trapezoidal sandwich porous/GPLR plates with respect to the influences of different porosity distributions and GPLs patterns. Explanation of the material properties of such nanocomposites accounting for porosity and GPLs reinforced content is performed via Halpin-Tsai micromechanical rule. The existing governing equations of the problem based on the FSDT in the Cartesian coordinate system are properly transformed into trapezoidal coordinate. The GDQ method is used for discretizing of governing equations at different B.Cs. Results of the present study are compared with existing results in the literature.

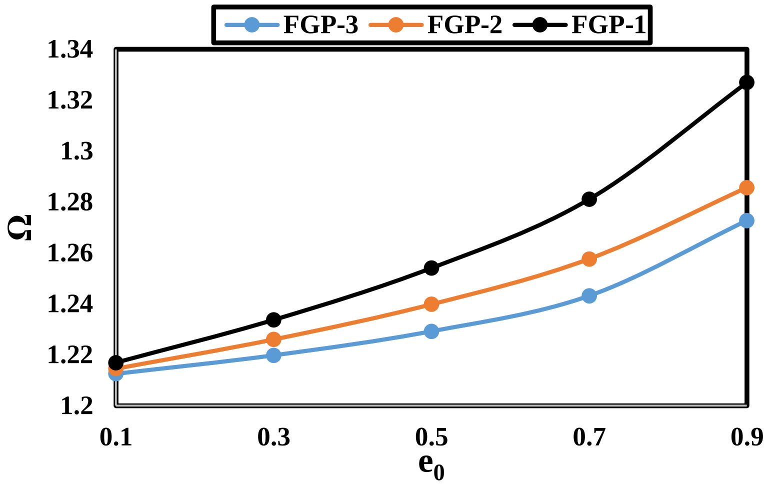

Fig. 8 Fundamental frequency parameter (Ω) of the CFCF trapezoidal sandwich plate with respect to various porosity coefficient e0 for different pattern of porosities

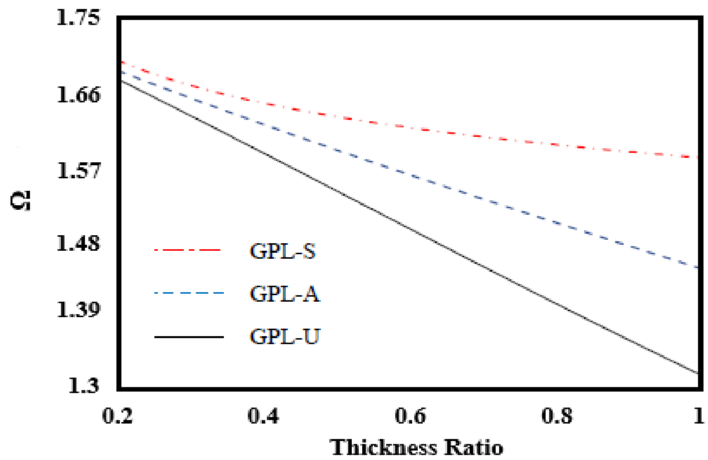

Fig. 9 Fundamental frequency parameter (Ω) of the CFSC trapezoidal sandwich plate with respect to various thickness ratio (h_f/h_c) for different reinforced pattern

The results reveal that

- Plates with higher GPL weight fraction and more GPLs dispersing near the top and bottom surfaces of the face sheets have higher natural frequencies.
- Reinforcing face sheets with GPL-S and FGP-2 pattern for metal core presents the highest fundamental frequency in valuation with other mixtures of GPLs and porosity distribution.
- In all three-porosity distribution, the fundamental frequency increases with increasing of porosity coefficient.
- It can be seen that the frequency parameter of the sandwich plate decrease with the increase of the thickness ratio.
- Fundamental frequency increases when the angle β increases. This indicates that the increase in bottom angle will increases the stiffness and natural frequency of the trapezoidal plate (Fig. 6).
- Results show that as the angle θ increased, dimensionless frequency reduced (Fig. 4).

According to the results for better understanding of mechanical behavior of nanocomposite plates, it is crucial to consider porosities inside the material structures.

References

Affdl Halpin, J.C. and Kardos, J.L. (1976), “The Halpin-Tsai equations: A review”, *Polym. Eng. Sci.*, **16**(5), 344-352. https://doi.org/10.1002/pen.760160512.

Afrookhteh, S.S., Fathi, A., Naghdipour, M. and Alizadeh Sahraei, A. (2016), “An experimental investigation of the effects of weight fractions of reinforcement and timing of hardener addition on the strain sensitivity of carbon nanotube/polymer composites”, *U.P.B. Sci. Bull., Series B*, **78**(4), 121-130.

Afrookhteh, S.S., Shakeri, M., Baniassadi, M. and Alizadeh Sahraei, A. (2018), “Microstructure reconstruction and

characterization of the porous GDLs for PEMFC based on fibers orientation distribution", *Fuel Cells*, **18**(2), https://doi.org/10.1002/fuce.201700239.
Arefi, M. (2015), "Elastic solution of a curved beam made of functionally graded materials with different cross sections", *Steel Compos. Struct.*, **18**(3), 659-672. https://doi.org/10.12989/scs.2015.18.3.659.
Barka, M., Benrahou, K.H., Bakora, A. and Tounsi, A. (2016), "Thermal post-buckling behavior of imperfect temperature-dependent sandwich FGM plates resting on Pasternak elastic foundation", *Steel Compos. Struct.*, **22**(1), 91-112. https://doi.org/10.12989/scs.2016.22.1.091.
Bennai, R., Ait Atmane, H. and Tounsi, A. (2015), "A new higher-order shear and normal deformation theory for functionally graded sandwich beams", *Steel Compos. Struct.*, **19**(3), 521-546. https://doi.org/10.12989/scs.2015.19.3.521.
Bert, C.W. and Malik, M. (1996), "Differential quadrature method in computational mechanics: a review", *Appl. Mech. Rev.*, **49**, 1-27. https://doi.org/10.1115/1.3101882.
Bouchafa, A., Bouiadjra, M.B., Houari, M.S.A. and Tounsi, A. (2015), "Thermal stresses and deflections of functionally graded sandwich plates using a new refined hyperbolic shear deformation theory", *Steel Compos. Struct.*, **18**(6), 1493-1515. https://doi.org/10.12989/scs.2015.18.6.1493.
Bouguenina, O., Belakhdar, K., Tounsi, A. and Bedia, E.A.A. (2015), "Numerical analysis of FGM plates with variable thickness subjected to thermal buckling", *Steel Compos. Struct.*, **19**(3), 679-695. https://doi.org/10.12989/scs.2015.19.3.679.
Chen, C.S., Liu, F.H. and Chen, W.R. (2017), "vibration and stability of initially stressed sandwich plates with FGM face sheets in thermal environments", *Steel Compos. Struct.*, **23**(3), 251-261. https://doi.org/10.12989/scs.2017.23.3.251.
Eyvazian, A., Hamouda, A.M., Tarlochan, F., Mohsenizadeh, S. and Ahmadi Dastjerdi, A. (2019), "Damping and vibration response of viscoelastic smart sandwich plate reinforced with non-uniform Graphene platelet with magnetorheological fluid core", *Steel Compos. Struct.*, **33**(6), 891-906. https://doi.org/10.12989/scs.2019.33.6.891.
Fantuzzi, N., Tornabene, F., Bacciocchi, M. and Dimitri, R. (2017), "Free vibration analysis of arbitrarily shaped functionally graded carbon nanotube-reinforced plates", *Compos. Part B*, **115**, 384-408. https://doi.org/10.1016/j.compositesb.2016.09.021.
Finot, M. and Suresh, S. (1996), "Small and large deformation of thick and thin-film multilayers: effect of layer geometry, plasticity and compositional gradients", *J. Mech. Phys. Solids*, **44**(5), 683-721. https://doi.org/10.1016/0022-5096(96)84548-0.
Gupta, A.K. and Sharma, S. (2014), "Free transverse vibration of orthotropic thin trapezoidal plate of parabolically varying thickness subjected to linear temperature distribution", *Shock and Vib.*, 2014, 1-6. http://dx.doi.org/10.1155/2014/392325.
Gupta, A.K. and Sharma, P. (2016), "Vibration study of non-homogeneous trapezoidal plates of variable thickness under thermal gradient", *J.V.C. Control*, **22**(5), 1369-1379. https://doi.org/10.1177/1077546314535280.
Gürses, M., Civalek, Ö., Ersoy, H. and Kiracioglu, O. (2009), "Analysis of shear deformable laminated composite trapezoidal plates", *Mater. Design*, **30**, 3030-3035. https://doi.org/10.1016/j.matdes.2008.12.016.
Haldar, S. and Manna, M.C. (2003), "A high precision shear deformable element for free vibration of thick/thin composite trapezoidal plates", *Steel Compos. Struct.*, **3**(3), 213–229.
Halpin, J.C. and Tsai, S.W. (1969), "Effects of environmental factors on composite materials", *AFML-TR*-67-423.
Houmat, A. (2001), "A sector Fourier p-element applied to free vibration analysis of sectorial plates", *J. Sound Vib.*, **243**(2), 269-282.
Kamarian, S., Shakeri, M., Yas, M.H., Bodaghi, M. and Pourasghar, A. (2015), "Free vibration analysis of functionally graded nanocomposite sandwich beams resting on Pasternak foundation by considering the agglomeration effect of CNTs", *J. Sandw. Struct. Mater.*, 1-31. https://doi.org/10.1177/1099636215590280.
Kapidzic, Z. (2013), "Strength analysis and modeling of hybrid composite-aluminum aircraft structures", Linkoping Studies in Science and Technology, Licentiate Thesis No. 1590.
Kettaf, F.Z., Houari, M.S.A., Benguediab, M. and Tounsi, A. (2013), "Thermal buckling of functionally graded sandwich plates using a new hyperbolic shear displacement model", *Steel Compos. Struct.*, **15**(4), 399-423. https://doi.org/10.12989/scs.2013.15.4.399.
Kim, C.S. and Dickinson, S.M. (1989), "On the free, transverse vibration of annular and circular, thin, sectorial plates subjected to certain complicating effects", *J. Sound Vib.*, **134**(3), 407-421. https://doi.org/10.1016/0022-460X(89)90566-X.
Kitipornchai, S., Chen, D. and Yang, J. (2017), "Free vibration and elastic buckling of functionally graded porous beams reinforced by graphene platelets", *Mater. Design*, **116**, 656-665. https://doi.org/10.1016/j.matdes.2016.12.061.
Koizumi, M. (1993), "The concept of FGM", *Ceram. Trans. Funct. Grad. Mater*., **34**, 3-10.
Liew, K.M. and Lam, K.Y. (1993), "On the use of 2-d orthogonal polynomials in the Rayleigh-Ritz method for flexural vibration of annular sector plates of arbitrary shape", *Int. J. Mech. Sci*., **35**(2), 129-139. https://doi.org/10.1016/0020-7403(93)90071-2.
Liew, K.M. and Liu, F.L. (2000), "Differential quadrature method for vibration analysis of shear deformable annular sector plates", *J. Sound Vib*., **230**(2), 335-356. https://doi.org/10.1006/jsvi.1999.2623.
Malekzadeh, P., Karami, G. (2005), "Polynomial and harmonic differential quadrature methods for free vibration of variable thickness skew plate", *Eng. Struct*., **27**, 1563-1574.
Marin, M., Agarwal, R.P. and Mahmoud, S.R. (2013), "Nonsimple material problems addressed by the Lagrange's identity", *Bound. Value Probl*., **2013**(1-14), 135.
Marin, M. and Florea, O. (2014), "On temporal behaviour of solutions in thermoelasticity of porous micropolar bodies", An. St. Univ. Ovidius Constanta, **22**(1), 169-188.
Marin, M. (1994), "The Lagrange identity method in thermoelasticity of bodies with microstructure', *Int. J. Eng. Sci.,* **32**(8), 1229-1240. https://doi.org/10.1016/0020-7225(94)90034-5.
Marin, M. and Nicaise, S. (2016), "Existence and stability results for thermoelastic dipolar bodies with double porosity", *Continuum Mech. Thermodynam.*, **28**(6), 1645-1657.
Marin, M., Ellahi, R. and Chirilă, A. (2017), "On solutions of Saint-Venant's problem for elastic dipolar bodies with voids", *Carpathian J. Mathematics*, **33**(2), 219-232.
Marin, M., Vlase, S., Ellahi, R. and Bhatti, M.M. (2019), "On the partition of energies for the backward in time problem of thermoelastic materials with a dipolar structure", *Symmetry*, Basel, **11**(7), 1-16.
Moradi-Dastjerdi, R. and Momeni-Khabisi, H. (2016), "Dynamic analysis of functionally graded nanocomposite plates reinforced by wavy carbon nanotube", *Steel Compos. Struct.*, **22**(2). https://doi.org/10.12989/scs.2016.22.2.277.
Moradi-Dastjerdi, R., Foroutan, M., Pourasghar, A. (2013), "Dynamic analysis of functionally graded nanocomposite cylinders reinforced by carbon nanotube by a mesh-free method", *Mater. Des*., **44**, 256-266. https://doi.org/10.1016/j.matdes.2012.07.069.
Mukhopadhyay, M. (1979), "A semi-analytic solution for free vibration of annular sector plates", *J. Sound Vib*., **63**(1), 87-95.
Mukhopadhyay, M. (1982), "Free vibration of annular sector

plates with edges possessing different degrees of rotational restraints", *J. Sound Vib*., **80**(2), 275-279. https://doi.org/10.1016/0022-460X(82)90196-1.

Park, W.T., Han, S.C., Jung, W.Y. and Lee, W.H. (2016), "Dynamic instability analysis for S-FGM plates embedded in Pasternak elastic medium using the modified couple stress theory", *Steel Compos. Struct.*, **22**(6), 1239-1259. https://doi.org/10.12989/scs.2016.22.6.1239.

Pelletier Jacob, L. and Vel Senthil,S. (2006), "An exact solution for the steady state thermo elastic response of functionally graded orthotropic cylindrical shells", *Int. J. Solid Struct*., **43**, 1131-1158. https://doi.org/10.1016/j.ijsolstr.2005.03.079.

Rajabi, J. and Mohammadimehr, M. (2019), "Hydro-thermo-mechanical biaxial buckling analysis of sandwich micro-plate with isotropic/orthotropic cores and piezoelectric/polymeric nanocomposite face sheets based on FSDT on elastic foundations", *Steel and Composite Structures, An Int'l Journal*, **33**(4), 509-523. https://doi.org/10.12989/scs.2019.33.4.509.

Ramaiah, G.K. and Vijayakumar, K. (1974), "Natural frequencies of circumferentially truncated sector plates with simply supported straight edges", *J. Sound Vib*., **34**(1), 53-61.

Rashad, M. and Yang, T.Y. (2018), "Numerical study of steel sandwich plates with RPF and VR cores materials under free air blast loads", *Steel Compos. Struct.*, **27**(6), 717-725. https://doi.org/10.12989/scs.2018.27.6.717.

Reddy J.N. (2013), "An Introduction to Continuum Mechanics", Second Edition, Cambridge University Press, 2013.

Sahla, M., Saidi, H., Draiche, K., Bousahla, A.A., Bourada, F. and Tounsi, A. (2019), "Free vibration analysis of angle-ply laminated composite and soft core sandwich plates", *Steel Compos. Struct.*, **33**(5), 663-679. https://doi.org/10.12989/scs.2019.33.5.663.

Saidi, H., Houari, M.S.A., Tounsi, A. and Bedia, E.A. (2013), "Thermo-mechanical bending response with stretching effect of functionally graded sandwich plates using a novel shear deformation theory", *Steel Compos. Struct.*, **15**(2), 221-245. https://doi.org/10.12989/scs.2013.15.2.221.

Salah, F., Boucham, B., Bourada, F. and Benzair, A. (2019), "Investigation of thermal buckling properties of ceramic-metal FGM sandwich plates using 2D integral plate model", *Steel Compos. Struct.*, **33**(6), 805-822. https://doi.org/10.12989/scs.2019.33.6.805.

Seok, J.W. and Tiersten, H.F. (2004), "Free vibrations of annular sector cantilever plates part 1: out-of-plane motion", *J. Sound Vib*., **271**(3-5), 757-772. https://doi.org/10.1016/S0022-460X(03)00414-0.

Setoodeh, A.R. and Shojaee, M. (2016), "Application of TW-DQ method to nonlinear free vibration analysis of FG carbon nanotube-reinforced composite quadrilateral plates", *Thin-Wall. Struct.*, **108**, 1-11. http://dx.doi.org/10.1016/j.tws.2016.07.019.

Sharma, K. and Marin, M. (2013), "Effect of distinct conductive an thermodynamic temperatures on the reflection of plane waves in micropolar elastic half-space", *Scientific Bulletin, Series A Appl.Math. Phys.*, **75**(2), 121-132.

Sharma, A., Sharda, H.B. and Nath, Y. (2005a), "Stability and vibration of Mindlin sector plates: an analytical approach", *AIAA J.*, **43**(5), 1109-1116. https://doi.org/10.2514/1.4683.

Sharma, A., Sharda, H.B. and Nath, Y. (2005b), "Stability and vibration of thick laminated composite sector plates", *J. Sound Vib*., **287**(1-2), 1-23. https://doi.org/10.1016/j.jsv.2004.10.030.

Shen, H.S. and Zhang, C.L. (2010), "Thermal buckling and postbuckling behavior of functionally graded carbon nanotube-reinforced composite plates", *Mater. Design*., **31**(7),3403-3411. https://doi.org/10.1016/j.matdes.2010.01.048.

Shokrollahi, S. and Shafaghat, S. (2016), "A global Ritz formulation for the free vibration analysis of hybrid metal-composite thick trapezoidal plates", *Scientia Iranica T. B: Mech. Eng*., **23**(1), 249-259.

Shu C., 2012, Differential Quadrature and its Application in Engineering, Springer Science & Business Media.

Sobhani Aragh, B., Nasrollah Barati, A.H. and Hedayati, H. (2012), "Eshelby–Mori–Tanaka approach for vibrational behavior of continuously graded carbon nanotube-reinforced cylindrical panels", *Compos. B Eng*., **43**(4), 1943-1954. https://doi.org/10.1016/j.compositesb.2012.01.004.

Tahouneh, V. (2016), "Using an equivalent continuum model for 3D dynamic analysis of nanocomposite plates", *Steel Compos. Struct.*, **20**(3), 623-649. https://doi.org/10.12989/scs.2016.20.3.623.

Tahouneh, V. (2017), "The effect of carbon nanotubes agglomeration on vibrational response of thick functionally graded sandwich plates", *Steel Compos. Struct.*, **24**(6), 711-726. https://doi.org/10.12989/scs.2017.24.6.711.

Torabi, K. and Afshari, H. (2017), "Vibration analysis of a cantilevered trapezoidal moderately thick plate with variable thickness", *Eng. Solid Mech.*, **30**(8), 71-92. https://doi.org/10.5267/j.esm.2016.7.001.

Tornabene, F. and Viola, E. (2008), "2-D solution for free vibrations of parabolic shells using generalized differential quadrature method", *Eur. J. Mech. A/Solids*, **27**, 1001-1025. https://doi.org/10.1016/j.euromechsol.2007.12.007.

Tornabene, F., Fantuzzi, N., Bacciocchi, M. and Viola, E. (2016), "Effect of agglomeration on the natural frequencies of functionally graded carbon nanotube-reinforced laminated composite doubly-curved shells", *Compos. Part B*, **89**, 187-218. https://doi.org/10.1016/j.compositesb.2015.11.016.

Tornabene, F., Fantuzzi, N. and Bacciocchi, M. (2017), "Linear static response of nanocomposite plates and shells reinforced by agglomerated carbon nanotubes", *Compos. Part B*., **115**, 449-476. https://doi.org/10.1016/j.compositesb.2016.07.011.

Tornabene, F., Fantuzzi, N., Ubertini, F. and Viola, E. (2015), "Strong formulation finite element method based on differential quadrature: A survey", *Appl. Mech. Rev*., **67**(2), 1-55. https://doi.org/10.1115/1.4028859.

Tornabene, F., Fantuzzi, N. and Bacciocchi, M. (2019), "Refined shear deformation theories for laminated composite arches and beams with variable thickness: Natural frequency analysis", *Eng. Anal. Bound. Elem*., **100**, 24-47. https://doi.org/10.1016/j.enganabound.2017.07.029.

Tornabene, F., Fantuzzi, N. and Bacciocchi, M. (2017), "Foam core composite sandwich plates and shells with variable stiffness: Effect of the curvilinear fiber path on the modal response", *J. Sandw. Struct. Mater*., **21**(1), 320-365. https://doi.org/10.1177/1099636217693623.

Wu, C.P. and Liu, Y.C. (2016), "A state space meshless method for the 3D analysis of FGM axisymmetric circular plates", *Steel Compos. Struct.*, **22**(1), 161-182. https://doi.org/10.12989/scs.2016.22.1.161.

Zamani, M., Fallah, A. and Aghdam, M.M. (2012), "Free vibration analysis of moderately thick trapezoidal symmetrically laminated plates with various combinations of boundary conditions", *Eur. J. Mech. A/Solids*, 36(2012), 204-212. https://doi.org/10.1016/j.euromechsol.2012.03.004.

Zhao, Z., Feng, C., Dong, Y., Wang, Y. and Yang, J. (2019), "Geometrically nonlinear bending of functionally graded nanocomposite trapezoidal plates reinforced with graphene platelets (GPLs)", *Int. J. Mech. Mater. Des*., **15**(4). https://doi.org/10.1007/s10999-019-09442-4.

Zhao, Z., Feng, C., Wang, Y. and Yang, J. (2017), "Bending and vibration analysis of functionally graded trapezoidal nanocomposite plates reinforced with graphene nanoplatelets (GPLs)", *Compos. Struct.*, **180**, https://doi.org/10.1016/j.compstruct.2017.08.044.

Zhu, X.H. and Meng, Z.Y. (1995), "Operational principle fabrication and displacement characteristics of a functionally gradient piezoelectricceramic actuator", *Sensor. Actuat.*, **48**(3), 169-176. https://doi.org/10.1016/0924-4247(95)00996-5.

CC